19th Australasian Fluid Mechanics Conference
Melbourne, Australia
8-11 December 2014

Experimental Investigation of Momentum Transport Associated with the Interaction of Concentrated and Distributed Vorticity

H. U. Ain[1], J. R. Elsnab[1] and J. C. Klewicki[1,2]

[1]Department of Mechanical Engineering
University of Melbourne, Parkville, VIC 3010, Australia

[2]Department of Mechanical Engineering
University of New Hampshire, Durham, New Hampshire 03824, USA

Abstract

The flow field associated with a vortex ring advecting towards a moving wall is investigated. These physical simulations represent aspects of instantaneous flow field interactions known to exist in turbulent wall bounded flows. To allow for an explicit study of these interactions and avoid background turbulence, unsteady, laminar, vortex ring experiments are conducted with reproducible initial conditions. The experiments are conducted in a large water tank. The shear layer is validated and the basic parameters associated with the vortex ring are quantified. Opposite sign vorticity interactions between the vortex ring and shear layer vorticity results in a lifting of the near wall fluid. This gives rise to the formation of a primary hairpin vortex with the same sign vorticity as the top core of the vortex ring. The evolution of the hairpin is consistent with observations noted in a turbulent boundary layer.

Introduction

Turbulent flows are of ubiquitous technological importance due to their wide variety of applications. The action of vortical motions plays a vital role in turbulence production, dissipation, and time-averaged turbulence statistics. Therefore, it is important to understand what flow features are responsible for the inertial mechanisms of turbulence and ultimately the mean distribution of momentum. A variety of experimental and numerical studies suggests the presence of distinct coherent regions existing within the vorticity field of the wall-bounded turbulent flows, which are commonly termed "hairpins," hp [1]. These coherent motions are thought to be the building block of wall-bounded turbulence and serve as a basis for modelling the turbulent boundary layer, e.g., see Smith et al. [9].

By convecting a vortex ring (Falco's *typical eddies*) towards or away from a moving wall, Chu and Falco [4] were able to investigate features that have been observed in the turbulent boundary layer using flow visualization. They have broadly classified these interactions (vortex ring/moving wall) based upon stability considerations into four types (see therein for details). Dupont et al. [5] used a similar experimental set-up to [4] but used advanced measurement techniques, e.g., particle image velocimetry (PIV), for detailed characterization of type II interactions. Their findings indicated that the vortex ring acted as an external perturbation, which resulted in the lift up of the shear-layer, thereby, producing a hairpin. The studies by Haidari and Smith [6] provide important clarity regarding asymmetries inherent in the generation and regeneration of hairpins e.g., vortices and their contribution towards turbulent inertia. They validated this by examining vortex dynamics near a wall in a well-controlled environment and established an extension of the results to the dynamics of a turbulent boundary layer. Their experimental studies described that the lasting contribution to the mean Reynolds stress (turbulent inertia) are made during events causing surface layer eruptions followed by roll up of sheets of vorticity and these events continue to occur repeatedly. Another important conclusion drawn from their analysis is that in high shear flows, a small amount of local asymmetry can give rise to much larger asymmetry for a single vortex or combination of vortices. This motivates the fact that those interactions that leave a signature on the mean dynamics must contain asymmetries associated with their geometry or kinematics. Bernard [3] numerically examined the vorticity field in a transitional boundary layer. The results suggests that shearing of spanwise vorticity beyond the viscous sublayer creates wall-normal vorticity away from the boundary. This effect causes the appearance of streamwise vorticity shaping into a hairpin.

Herein, we report on experiments investigating velocity-vorticity interactions that underlie the dynamical mechanisms by which turbulent motions distribute momentum. The scope of this study is to examine the growth and evolution of the resulting hairpin relative to an advecting vortex ring. It is an extension of the Dupont et al. [5] study since they were not able to characterize the properties of the hairpin. The aim of the study is to clarify specific properties of the hairpin, e.g., spanwise vorticity, trajectory, and circulation in the hairpin core. It is thought that by understanding the details of this interaction, further insight can be gained into the generic mechanisms operative in wall-bounded turbulent flows and vorticity dynamics in general.

Experimental Facility

Vortex rings are generated using a 127 mm piston-cylinder device and a 34.8 mm seamless stainless steel tube. The cylinder and tube are connected using flexible tubing. The piston-cylinder motion is precisely controlled using LabView and a stepper motor. A vortex ring is produced at the exit of the tube by converting rotational motion from the stepper motor to translation using a threaded rod. The outer contour at the exit plane of the tube is machined to form a wedge with a 10° tip angle and length of 6 mm. A Stokes layer, also referred to as the Rayleigh problem, i.e., a time developing shear-layer, is generated using a conveyor belt that is 305 mm wide and 1.83 m long. The conveyor belt rides on a nominally flat acrylic plate and is driven by a servo motor/timing belt system. Trapezoidal velocity versus time profiles are implemented in LabView with an impulse configuration, i.e., acceleration time is much less than the overall time interval, T. Since

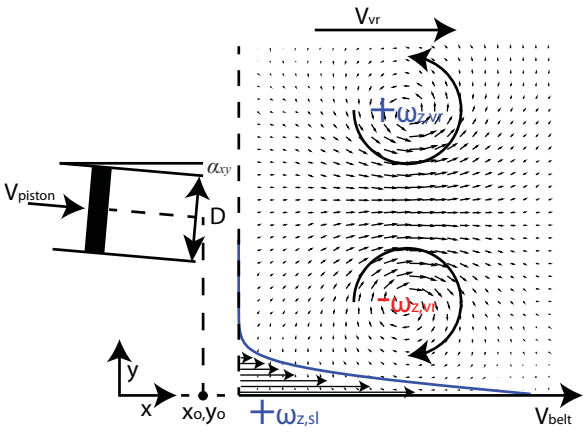

Figure 1. Schematic of a vortex ring interacting with a shear-layer. x_o, y_o is the global origin.

the acceleration time of the shear-layer is $\ll 1$ second, the belt can be considered impulsively started. As time, t, increases, a laminar Stokes layer bearing the spanwise vorticity generated during startup diffuses normal to the conveyor belt. Note that even if one does not consider the belt impulsively started, the amount of vorticity in the layer, i.e., its circulation, is equivalent. The conveyor belt continually operates until the vortex ring passes through the field of view. Also note that the Stokes layer thickness scales with $\sqrt{t}$. Thus, the layer thickness is essentially constant as the ring advects through the field of view since the total image acquisition time is less than 5 seconds and the time delay between the shear-layer startup and vortex ring generation is > 20 seconds. The belt velocity, V_b ranges from $7.95 - 9.55$ cm/sec and propagates in the same direction as the vortex ring. This provides the opportunity to explore opposite sign vorticity interactions between the bottom lobe of the vortex ring and shear layer. Rotation of the vortex generator tube in the $x-y$ plane, α_{xy}, is accomplished using a precision rotation stage and is verified using a precision digital level. The vortex generator and conveyor belt are used in a large water tank with width of 1.08 m, length of 3.6 m and height of 0.37 m. The glass tank is filled with water maintained at a constant water level to ensure constant hydrostatic pressure. Vortex rings are formed using a stroke length, L/D of 2.0, where L is the fluid displacement in the tube and D is the tube diameter, at a Reynolds number based upon average slug velocity, $\overline{V_s} = 1/T \int v_s(t)dt$ and tube diameter of 2500 and 2972. A schematic of the interaction is presented in figure 1.

Data Acquisition

Quantitative information about the instantaneous flow field is obtained using digital particle image velocimetry. A standard planar PIV system is utilized and images are acquired using a CCD camera with resolution 4072 x 2720 $pixel^2$. A double-pulsed Nd:YAG laser operating at 532 nm is used as the light source. Synchronization between the CCD camera and laser Q-switch timing is obtained using pulse generators. The water tank is seeded with hollow glass sphere particles, nominally 15 microns in diameter. The image pairs are captured at a rate of 2 Hz. The time delay, Δt, between image capture ranges from 3.5 to 4.5 ms to ensure that the particle displacement does not exceed 8 to 10 pixels. The pulse generator issues an output signal to trigger LabView that synchronizes the start up of the shear-layer belt and the generation of the vortex ring. The accuracy of synchronization is limited to 0.001 s since the timing is achieved using software.

Case	$Re_{vr} = \overline{V_s}D/\nu$	$Re_{sl} = \delta^* V_b/\nu$	ζ_{sl}/ζ_{vr}	α°_{xy}
1, ◇	2500	492	0.69	3
2, □	2972	492	0.58	3
3, ○	2972	444	0.83	3
4, ◁	2972	492	0.58	0

Table 1. Experimental parameters and symbols for the investigated scenarios, where δ^* is the displacement thickness, sl is the shear-layer, and vr is the vortex ring. The formation circulation, based upon a slug model, for the vr is $\overline{V_s}2D$ and for the sl, $V_b D_c$, where D_c is the distance between the vr cores and ν is the kinematic viscosity.

Data Reduction

For post processing of the PIV images, a multi-pass, multigrid, cross-correlation algorithm is utilized [2]. A base interrogation window size of 32 x 32 $pixel^2$ is utilized in the first pass, which is subsequently followed by a window size of 16 x 16 $pixel^2$ with 50% overlap in the second pass. Due to the presence of large velocity gradients, the measurement of the velocity field is subject to larger uncertainty and a greater vector rejection rate. Therefore, a window deformation scheme [8] is used in conjunction with the multigrid scheme. The field of view starts $2/3D$ from the vortex generation tube and the centreline of the tube is $1.5D$ from the conveyor belt in the wall-normal direction for all cases investigated. The PIV field of view is $5.6D$ x $3.8D$ and is centred on the wall-normal plane of symmetry of the ring. The spatial resolution of velocity vectors in both the streamwise and wall-normal directions is $0.011D$. The instantaneous velocity vector fields are phase and conditionally averaged on the location of the maximum spanwise vorticity to determine the characteristics of the vortex ring alone. The hairpin characteristics are analyzed by phase and conditional averaging the peak spanwise vorticity location for the hairpin. This spatial averaging is employed for 100 instantaneous realizations. Results presented are representative for either the vortex ring or hairpin. The conditional averaging is employed to correct for the random Gaussian modulation of vortex trajectory, referred to as vortex wandering [7]. The spanwise vorticity, ω_z, is obtained by differentiating the velocity field using a least-squares method. The circulation, ζ, on the upper and lower half of the ring as well as the hairpin is obtained by Stokes theorem, $\equiv \oint_c u.dl = \int_A \omega_z dA$, using a two-dimensional version of the trapezoidal rule.

Results and Discussion

The Stokes layer is a finite thickness vortex sheet that is perturbed by the vortex ring, which subsequently forms the hairpin. Shear-layer results are shown in figure 3 for $Re_{sl} = 492$. The experimental profile is in good agreement with the analytical solution. Experimental parameters and symbol definition for the various cases are presented in table 1.

The trajectory of the vortex cores, i.e., locations of the minimum and maximum $\omega_{z,vr}$ and $\omega_{z,hp}$, are shown in figure 4. The 0° case trajectory bends further away from the wall in comparison to the 3° case. This is attributed to a decreased interaction between the shear layer and vortex ring, i.e., hairpin liftup is not hindered by the bottom lobe of the vortex ring. However, the vortex ring is drawn away from the wall for all interactions. This apparent lift

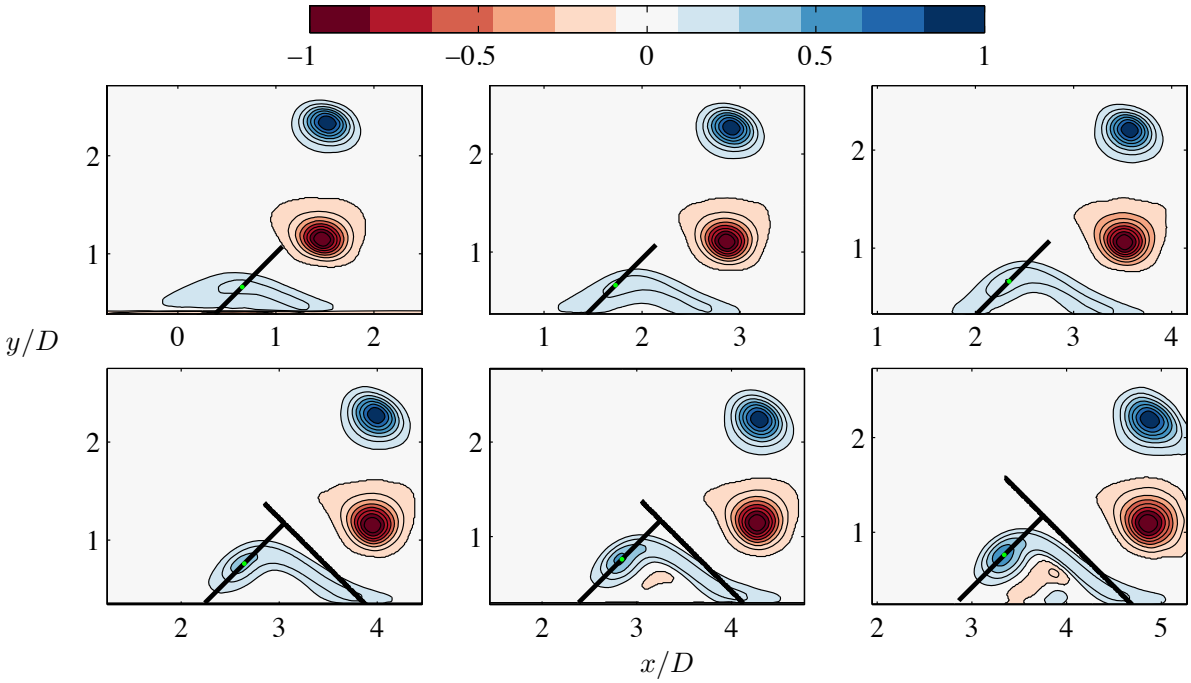

Figure 2. Contours of the conditionally averaged spanwise vorticity for case 1 normalized with $\omega_{z,vr,max}$. The vortex ring is travelling from left to right. The solid lines are at 45° and the ● is the location of $\omega_{z,hp,max}$.

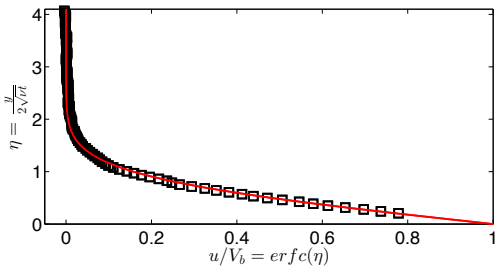

Figure 3. Comparison between the experimental shear-layer results and the analytical solution at Re_{sl} = 492. Description: □, experimental and red line, analytical.

force is attributed to an interaction between the opposite sign circulation in the bottom lobe of the ring and that of the hairpin since the circulation in the top and bottom lobes of the vortex ring essentially remains constant. The bottom core of the vortex ring is simply acting as a perturbation to the vortex sheet, hence, the bottom lobe circulation does not change since it is an inviscid interaction. The circulation of the bottom/top lobes and hairpin is presented in figure 5. The circulation of the hairpin approaches 80% of the top core. Analytically, the circulation per unit length in the shear-layer is simply the belt speed. If the characteristic length is taken to be the distance between the bottom and top cores of the ring, the total circulation in the hairpin is about 90% of the shear-layer. However, when the core of the hairpin starts to pinch, the circulation is reduced to around 60 – 70% of the top core. The circulation of the new lobe (from the head of the hairpin) is estimated by considering only spanwise vorticity that is greater than $2/3\omega_{z,hp,max}$. This criterion is arbitrary, but consistent, and is based upon yielding contours that do not include a vorticity contribution from the base of the hairpin. The evolution of the hairpin head circulation, which is representative of the new lobe formed after pinchoff, is approximately 15%. Conceptually, this is approximately the net transport of concentrated vorticity from the distributed vorticity to the free-stream since the remainder is simply advected downstream in the shear-layer. The peak vorticity in the vortex ring and hairpin exhibit different trends, which are shown in figure 6. Due to diffusion, the peak vorticity in the vortex ring decays. However, for the hairpin, the peak vorticity increases and then starts to decrease. The maximum ω_z in the hairpin is on the order of the Stokes profiles. Interestingly, the $\alpha_{xy} = 0$, case 4, has the highest vorticity level in the hairpin relative to that in the Stokes layer. It is not currently clear at this point why this is the case since one would expect a stronger interaction if the ring is directed towards the wall.

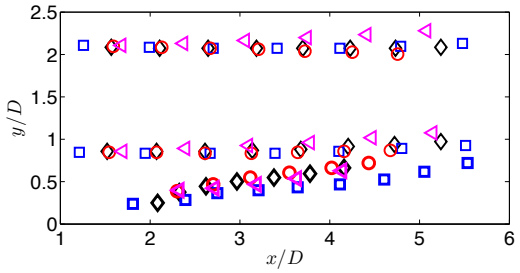

Figure 4. Trajectory of the min and max ω_z for the vortex ring and hairpin cores. Description: see table 1 for symbol definition and thick marker, hairpin

Contours of the hairpin evolution from a perturbed state to a developed state are presented in figure 2 for case 1. Since the hairpin and vortex ring do not interact, this is a so-called type II interaction [4]. The data are based upon a conditional average of the hairpin peak vorticity location. Note that the vortex ring contours are slightly smeared due to the conditional average on the hairpin location. Since data are obtained on the center-plane of the ring, there is no 'hairpin leg.' At a developed state, the head of the hairpin is oriented 45°. The peak contours in figure 2 are elliptical at both early and late x/D. This allows one

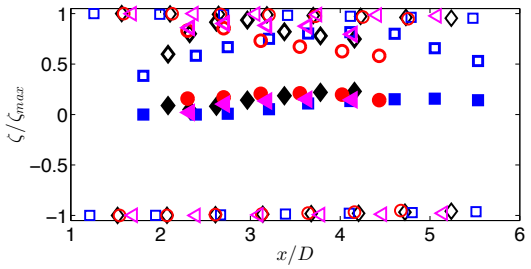

Figure 5. Circulation ratio in the vortex ring and hairpin normalized by the maximum $\zeta_{vr,max}$. Description: see table 1 for symbol definition; thick marker, hairpin; filled symbols, conditional average on $\omega_{z,hp} > 2/3\omega_{z,hp,max}$

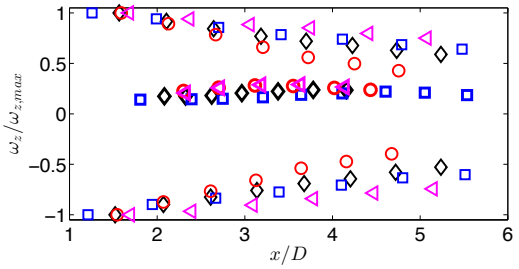

Figure 6. Spanwise vorticity in the vortex ring and hairpin normalized by the maximum $\omega_{z,vr,max}$. Description: see table 1 for symbol definition and thick marker, hairpin

to obtain the evolution angle of the hairpin by fitting an ellipse to the peak vorticity contour that is greater than $2/3\omega_{z,hp,max}$ and then determining the rotation angle with respect to the x-axis. The rotational angle of the ellipse is presented in the figure 7. At early x/D locations, the angle of the peak contour is aligned with velocity gradient in the shear layer, i.e., $\theta_{xy} < 0$. As the hairpin lifts, the angle continually increases to approximately 45°. When the head of the hairpin is pinched, the orientation is lost since the contour becomes nearly circular. These results are consistent with other kernel studies, e.g., [4, 5, 6]and results evident in the turbulent boundary layer [1].

The ω_z contours for the other cases are similar to those shown in figure 2. Initially, there is weak organization of the spanwise vorticity in the shear-layer. Depending upon the ratio of ζ_{sl}/ζ_{vr}, the organization occurs very quickly ($\zeta_{sl}/\zeta_{vr} > 0.8$) or tends to propagate in the streamwise direction before starting to rise. The liftup occurs until the head of the hairpin is oriented at a 45° and then subsequently pinches off. If $\zeta_{sl}/\zeta_{vr} = 0.35$, there is not sufficient perturbation to the shear-layer to form a hairpin, i.e., only a weak organization of spanwise vorticity. For circulation ratios greater than 1, the interaction is too strong to obtain conditionally averaged statistics, i.e., more of a type III interaction discussed in [4].

Conclusions

An experimental investigation on the formation, evolution and characteristics of a hairpin is reported. The results indicate that a hairpin generated through the interaction of a vortex ring and shear-layer are similar to that of a turbulent boundary layer. Furthermore, the results are consistent with other kernel studies who have commented on the formation of hairpins. It is thought that the optimal angle for the hairpin in terms of stability is $\approx 45°$ since the head of the hairpin is pinched for angles $\gtrsim 45°$.

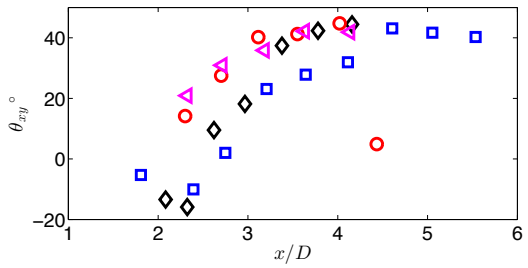

Figure 7. Rotation angle of the ellipse for the peak $2/3\omega_{z,hp,max}$ contour.

Acknowledgements

The authors gratefully acknowledge financial support provided by the Australian Research Council, grant number DP110102896.

References

[1] Adrian, R. J., Hairpin vortex organization in wall turbulencea, *Physics of Fluids*, **19**, 2007, 041301–041301.

[2] Adrian, R. J. and Westerweel, J., *Particle image velocimetry*, Cambridge University Press, 2011.

[3] Bernard, P. S., Boundary layer vorticity and the rise of hairpins, *Lille Workshop; Progress in wall turbulence: understanding and modelling*, 2014, P13.

[4] Chu, C. and Falco, R., Vortex ring/viscous wall layer interaction model of the turbulence production process near walls, *Experiments in Fluids*, **6**, 1988, 305 – 315.

[5] Dupont, P., Croisier, G., Werquin, O. and Stanislas, M., DPIV, HPTV and visualization study of a vortex ring–moving wall interaction, *Experiments in fluids*, **33**, 2002, 555–564.

[6] Haidari, A. H. and Smith, C. R., The generation and regeneration of single hairpin vortices, *Journal of Fluid Mechanics*, **277**, 1994, 135–162.

[7] Jammy, S., Hills, N. and Birch, D. M., Boundary conditions and vortex wandering, *Journal of Fluid Mechanics*, **747**, 2014, 350–368.

[8] Scarano, F. and Riethmuller, M. L., Advances in iterative multigrid PIV image processing, Tiergartenstrasse 17, Heidelberg, D-69121, Germany, 2000, volume 29, S51 – S60, S51 – S60.

[9] Smith, C., Walker, J., Haidari, A. and Sobrun, U., On the dynamics of near–wall turbulence, *Phil Trans. Phys. Sci and Eng.*, **336**, 1991, 131–175.